Exploring magnetism and magnetoelectric properties in the green phase of R_2BaCuO_5 (R = Er, Eu, Y, Tm, and Lu): The role of $4f$-$3d$ exchange coupling

Premakumar Yanda,[1] N. Boudjada,[2] Juan Rodríguez-Carvajal,[3] and A. Sundaresan[1]

[1]*School of Advanced Material, and Chemistry and Physics of Materials Unit, Jawaharlal Nehru Centre for Advanced Scientific Research, Bengaluru 560064, India*

[2]*Université Grenoble Alpes, Centre national de la recherche scientifique (CNRS), Institut Néel, 38000 Grenoble, France*

[3]*Institut Laue-Langevin, Diffraction Group, 71 Avenue des Martyrs, CS 20156, 38042 Grenoble Cedex 9, France*

(Received 2 November 2023; revised 9 January 2024; accepted 23 February 2024; published 12 March 2024)

We report a comprehensive investigation into the magnetic and magnetoelectric characteristics of green phase compounds R_2BaCuO_5 (R = Er, Eu, Y, Tm, and Lu) through an array of experimental techniques, including dc magnetization, specific heat, dielectric, pyrocurrent, and neutron diffraction measurements. Our study reveals that all these compounds exhibit antiferromagnetic ordering of Cu^{2+} ions in the range T_N^{Cu} = 15–20 K. Specifically, magnetic ordering of Er^{3+} ions is observed at T_N^{Er} = 5.1 K. Intriguingly, independent ordering of Tm^{3+} ions is not observed. Furthermore, the isothermal magnetization curves for the Er compound confirm the metamagnetic transition at a critical magnetic field of H_c = 0.9 T, reaching a saturation magnetization value of 9 μ_B/f.u. Notably, above H_c, this compound exhibits field-induced magnetoelectric states at T_N^{Er}, underscoring a pronounced magnetoelectric coupling. Conversely, the compounds with R = Eu, Y, Tm, and Lu do not display magnetoelectric coupling. The presence or absence of such coupling aligns with the magnetic symmetry derived from neutron diffraction. Our findings conclusively establish that $4f$-$3d$ exchange coupling is pivotal in enabling the magnetoelectric or multiferroic properties in these well-established green phase compounds. Consequently, our study underscores the rich and diverse magnetism and magnetoelectric properties exhibited by the green phase family, positioning them as equally intriguing as manganites in condensed matter physics.

DOI: 10.1103/PhysRevB.109.104411

I. INTRODUCTION

The intricate interplay between spin and lattice dynamics holds a fascination within condensed matter research, both for the captivating physics it unveils and its potential applications in memory and spintronic devices. Over the past two decades, magnetoelectric and multiferroic materials have been a focal point of extensive investigation [1–5]. Despite well-established foundations in this field, the quest for novel multiferroic materials remains a formidable challenge. Recently, insights have illuminated a pathway to magnetoelectric coupling through the interplay of $4f$-$3d$ coupling [6,7], introducing a novel dimension to this pursuit. Notably, the family of green phase compounds R_2BaCuO_5 (where R ranges from Sm to Lu, including Y) has emerged as a captivating arena for exploration, showcasing not only intriguing magnetic properties but also manifestation of magnetoelectric coupling arising from the intricate $4f$-$3d$ interaction [6–12].

The green phase family of compounds R_2BaCuO_5 (R = Sm–Lu, Y) was found as secondary phases in the early days of the synthesis of high-temperature $RBa_2Cu_3O_7$ superconductors. The crystal structure of these compounds was first solved by the Michael *et al.* showing that they crystallize in centrosymmetric orthorhombic *Pnma* structure [13]. Later, this structure has been confirmed by single crystal and neutron diffraction studies by different researchers [14,15]. In this structure, there are three cation sites (R1, R2, and Cu). When the R ions are magnetic, the interaction between d-d, f-f electrons, and, most importantly, f-d electrons results in fascinating magnetic properties [16–20]. Many of these compounds exhibit two magnetic phase transitions with unusual magnetic structures. The magnetic properties of these compounds have been well studied by different techniques such as magnetic measurements, ESR, Mössbauer, and neutron diffraction experiments [17,19–23].

Recently, it has been demonstrated that certain green phase compounds exhibit strong magnetoelectric coupling, stemming from magnetic structures determined by the interplay of $4f$-$3d$ coupling. Sm_2BaCuO_5 exhibits linear magnetoelectric effect below Cu^{2+} spins ordering temperature T_N^{Cu} = 23 K [8,9] and influenced further by the ordering of Sm^{3+} spins at T_N^{Sm} = 5 K. Interestingly, the isostructural compound Gd_2BaCuO_5 exhibits multiferroic properties below T_N = 11.9 K where Cu^{2+} and Gd^{3+} spins order simultaneously [6]. Further, this compound shows a lock-in phase transition from incommensurate to commensurate with additional polarization at T_{loc} = 6 K [6,24]. A neutron diffraction study has revealed the presence of an elliptical cycloidal magnetic structure with magnetic symmetry $P2_1ma1'(0,\ 0,\ \gamma)0s0s$ below T_N, which is responsible for the multiferroicity. Further, Dy_2BaCuO_5 and Ho_2BaCuO_5 compounds exhibit magnetoelectric coupling, which is consistent with the magnetic symmetry $mm'm$ and $2'/m$, respectively [7]. Therefore, it will be very intriguing to study other members of the family, including the nonmagnetic R ions to understand the role of $4f$-$3d$ coupling.

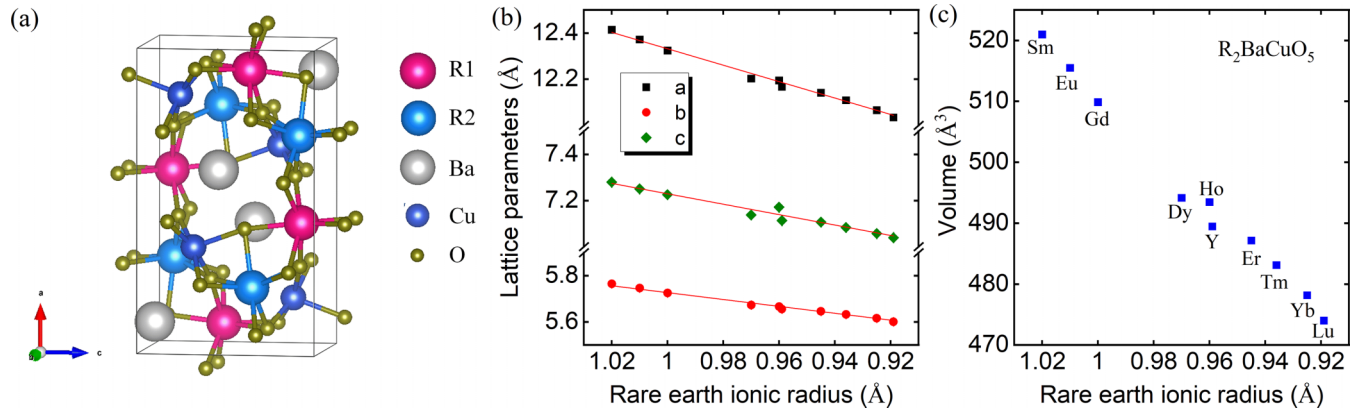

FIG. 1. (a) Crystal structure of R_2BaCuO_5 where R is rare-earth metal ion. (b) Lattice parameters with Vegard's law fitting and (c) Unit cell volume with respect to rare earth ionic radius.

In this paper, we present a comprehensive analysis of the magnetic and magnetoelectric properties of centrosymmetric R_2BaCuO_5 with R = Er, Eu, Y, Tm, and Lu. All these compounds exhibit antiferromagnetic ordering of Cu^{2+} ions in the range $T_N^{Cu} \sim$ 15–20 K. Notably, Tm^{3+} ions do not display magnetic ordering down to 2 K. Er^{3+} ions in Er_2BaCuO_5 undergo magnetic ordering at $T_N^{Er} = 5.1$ K and a metamagnetic transition is observed above the critical field of $H_c \sim 0.9$ T. Above H_c, we observed field-induced electric polarization around $T_N^{Er} = 5.1$ K. However, magnetoelectric coupling is conspicuously absent in the remaining compounds. The absence of magnetoelectric coupling at the magnetic ordering in zero applied magnetic field is consistent with our neutron diffraction measurements. Our study on Y_2BaCuO_5 and Lu_2BaCuO_5 reveal a nearly collinear magnetic structure (BNS: P_a2_1/c) with propagation vector (0, ½, ½) and R_2BaCuO_5 (R = Er and Tm) exhibits a noncollinear magnetic order (BNS: P_b112_1/n) with k vector (0, ½, 0). These ground state magnetic structures are all centrosymmetric and hence the absence of magnetoelectric coupling at $H = 0$ T.

II. EXPERIMENT

Polycrystalline samples of R_2BaCuO_5 (R = Er, Eu, Y, Tm, and Lu) were made under conventional solid-state route. Stoichiometric amounts of R_2O_3, $BaCO_3$, and CuO were mixed homogeneously and heated at 950 °C for 12 h. Our attempts to make Tb_2BaCuO_5 was not successful due to the formation of the stable phase $BaTbO_3$. Phase purity was checked by using PANalytical empyrean x-ray diffractometer with monochromatic Cu-Kα radiation. Neutron diffraction experiments were carried on D1B diffractometer at ILL with wavelength 2.52 Å. We have used FULLPROF for the analysis of x-ray and neutron powder diffraction data [25]. Diffuse reflectance spectra of powder samples were recorded using a Perkin-Elmer Lambda 900 spectrometer. Background correction was performed by subtracting prerecorded reflectance spectra of a $BaSO_4$ disc from the compound spectra. Direct current magnetization measurements were carried out in SQUID magnetometer, Quantum Design, USA. Specific heat was measured in physical property measurement system (PPMS), Quantum Design, USA. Dielectric and pyrocurrent measurements were carried out by using Agilent E4980A LCR meter and Keithley electrometer while temperature and magnetic field control provided by PPMS. We have obtained the electric polarization by integrating the pyrocurrent with respect to time.

III. RESULTS AND DISCUSSION

A. Crystal structure

The Rietveld refined x-ray diffraction and the obtained structural parameters for R_2BaCuO_5 (R = Er, Eu, Y, Tm, and Lu) at room temperature are provided in Figs. S1 and S2 and Tables SI-SV, respectively [26]. All the titled compounds crystallize in orthorhombic structure with space group *Pnma* as reported earlier [13]. This structure is centrosymmetric and does not allow ferroelectric properties. Figure 1 depicts the crystal structure and the variation of lattice parameters for all the green phase compounds with R-ion ionic radii. Going from Sm to Lu, as the ionic radii decrease (lanthanide contraction), the lattice parameters and the volume of the unit cell decrease linearly in agreement with Vegard's law. It should be noted that the compound Tb_2BaCuO_5 does not form because of thermodynamically competing stable phase of $BaTbO_3$. In this structure, R ions have two nonequivalent sites ($R1$ and $R2$) in Wyckoff position 4c with .m. site symmetry. Both sites are heptacoordinated by O^{2-} anions. The $R1O_7$ and $R2O_7$ capped prisms connected by common trigonal face into to $R1R2O_{11}$ units, which shares edges to form a three-dimensional network. The Cu^{2+} ions are in unusual oxygen square pyramids, which are isolated from each other so that there are no direct Cu-O-Cu bonds. The $R1$ ion is connected, through oxygens, to three copper ions with a bond angle close to 90°. Whereas $R2$ ion is surrounded by six copper ions through oxygen and five out of the six bonds are close 180°. Thus, copper molecular fields at both R sites are different and making the compound highly anisotropic. UV-Vis spectra of all the compounds that was collected in reflectance mode is shown in Fig. S3 [26]. All these compounds give a strong reflectance peak in the green range of 519–542 nm, which belongs to strong *d-d* transition of CuO_5 square pyramid. Therefore, these samples are green in color and hence they are called green phases. The corresponding bandgap ranges from 2.2–2.4 eV, which is in semiconducting region.

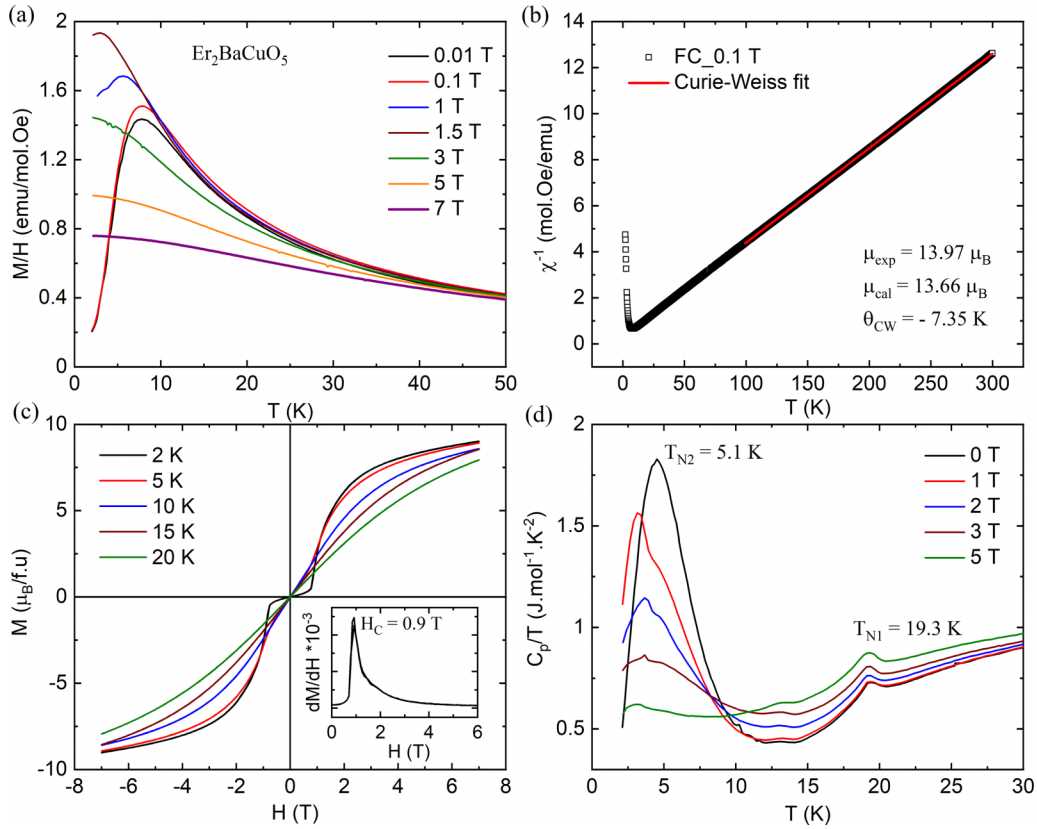

FIG. 2. (a) Temperature-dependent magnetization measured under different magnetic fields in field-cooled sequence. (b) Inverse susceptibility data for magnetic field 0.1 T along with Curie-Weiss fitting. (c) Isothermal magnetization curves were recorded at different temperatures. Inset shows the dM/dH curve at 2 K. (d) Specific heat data measured at different magnetic fields; for Er_2BaCuO_5.

B. Field-induced magnetoelectric states in Er_2BaCuO_5

Direct current magnetization and specific heat measurements for Er_2BaCuO_5 are presented in Fig. 2 and Fig. S4 [26]. As shown in Fig. 2(a), the magnetic susceptibility reveals an anomaly around 5.1 K due to independent ordering of Er^{3+} ions. However, we did not observe any anomaly for Cu^{2+} ordering due to dominant paramagnetic moment of Er^{3+} ions. The effective magnetic moment obtained from the Curie-Weiss fit to inverse susceptibility data in high-temperature region [Fig. 2(b)] is 13.97 μ_B, which agrees with the spin-only value 13.66 μ_B for both Er^{3+} and Cu^{2+} ions. The negative sign of the Curie-Weiss temperature $\theta_{CW} = -7.35$ K indicates that antiferromagnetic interactions are dominant. As the magnetic field increases, the magnetic anomaly became broad and suppressed, suggesting a possible change in magnetic structure. Moreover, isothermal magnetization curves shown in Fig. 2(c) reveal a metamagnetic transition at the critical field $H_c = 0.9$ T and below T_N^{Er}. Below H_c, the curves are linear as expected for the antiferromagnetic ordering. At high magnetic fields ~7 T, this compound exhibits ferromagnetic behavior with a large magnetization of value ~9 μ_B/f.u., which is close to saturation. Further, the long-range magnetic ordering confirmed by specific heat measurements is shown in Fig. 2(d). As seen from the figure, it exhibits antiferromagnetic ordering of Cu^{2+} spins at $T_N^{Cu} = 19.3$ K and Er^{3+} moments at $T_N^{Er} = 5.1$ K. However, under applied magnetic fields, the spin structure below T_N^{Cu} looks quite insensitive to field but the structure below T_N^{Er} shows a significant change.

To know the ground-state magnetic structure, we have carried out neutron diffraction measurements on polycrystalline samples of Er_2BaCuO_5. As can be seen from the Fig. S5, there are new reflections below T_N^{Cu} confirming the long-range magnetic ordering [26]. We found that the **k** vector is (0, ½, 0) below T_N^{Cu}, which remains unchanged down to 1.5 K. The observed **k** vector is same as that of high-temperature magnetic phase of Dy_2BaCuO_5 and Ho_2BaCuO_5. We have used ISODISTORT to find out the possible magnetic solutions [27]. There are two two-dimensional (2D) irreps namely mY1 and mY2, with order parameters of the form (a, 0), (a, a), and (a, b), which gives the six possible magnetic models for the **k** vector (0, ½, 0) and the paramagnetic space group *Pnma*.1'. We have tried the highest symmetry models to fit our experimental data and found that P_b112_1/n in BNS notation (standard setting: P_a2_1/c in BNS or $P2_1/c.1'_a[P2_1/c]$ in the newly introduced UNI notation [28]. The transformation from our setting to the standard is: b, –c, –a –b; 0, 0, 0) is the correct solution obtained for the irrep mY1(a, a). The refinement of data at 1.5 K is shown in Fig. S6 and the resulting structural parameters of the refinement and the obtained magnetic structure can be found in the file Er_2BaCuO_5.mcif provided as Supplemental Material [26]. The corresponding magnetic structure at 1.5 K is shown in Fig. 3(a) and the structure

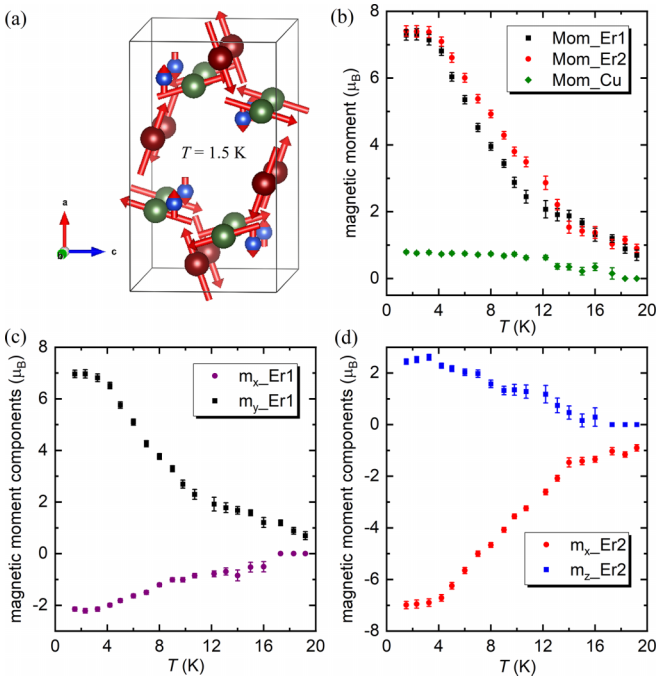

FIG. 3. (a) Magnetic structure of Er_2BaCuO_5 at 1.5 K. Er1 (green), Er2 (wine), and Cu (blue). (b) Temperature evolution of magnetic moments of Er1, Er2, and Cu. (c), (d) Magnetic moment components behavior with temperature of the Er1 and Er2 atoms.

is strongly noncollinear. Figure 3(b) shows the temperature evolution of magnetic moments of all three ions and their magnetic components in Figs. 3(c) and 3(d), as indicated in the figures. It is clear from the Fig. 3(b) that the Er moments in the range $T_N^{Er} \leqslant T \leqslant T_N^{Cu}$ behave like an induced moment by Cu spins. Below T_N^{Er}, the Er moment saturated where Er^{3+} moments order independently. In contrast to Dy and Ho compounds, the **k** vector is stable down 1.5 K indicates the role of single-ion rare-earth anisotropy and $4f$-$3d$ coupling in the formation of the magnetic ground state [7]. This magnetic point symmetry $2/m.1'$ is centrosymmetric, and this implies a null magnetoelectric tensor.

Further, we have carried out dielectric and pyrocurrent measurements to reveal magnetodielectric effect or multiferroicity. The obtained dielectric measurements results are displayed in the Fig. 4(a). We did not observe any dielectric anomaly at both Cu- and Er-ordering temperatures at low magnetic fields. Interestingly, a dielectric anomaly appears at T_N^{Er} under applied magnetic fields above $H_c > 0.9$ T. This compound exhibit magnetodielectric effect of 0.12% at 2 K and 9 T as seen from the Fig. 4(b). The isothermal magnetodielectric curves shows anomalies indicating multiple metamagnetic transitions. We have carried out pyrocurrent measurements to check whether the field-induced dielectric anomaly is associated to magnetoelectricity or not. Temperature and magnetic field variation of pyrocurrent data are shown in Fig. 4(c). In accordance with the centrosymmetric magnetic symmetry by the neutron diffraction, we did not observe electric polarization at 0 T. Interestingly, this

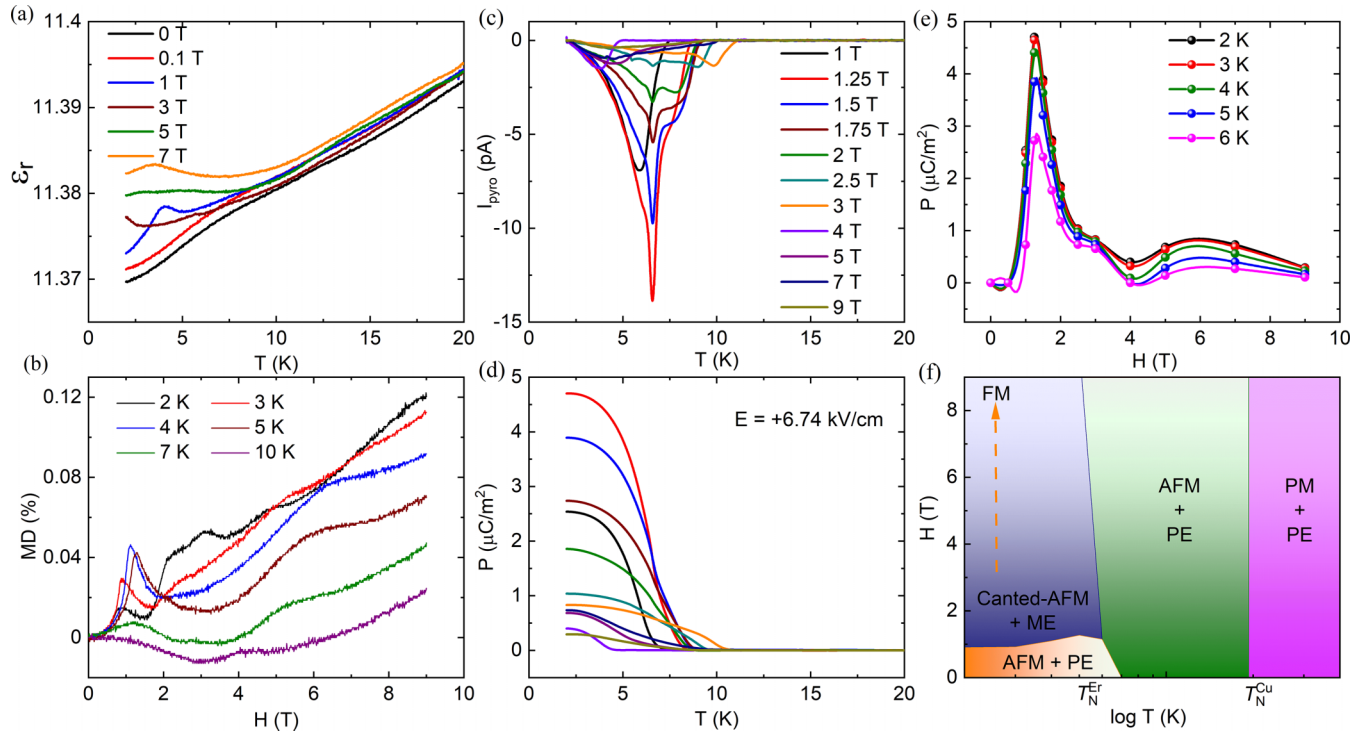

FIG. 4. (a) Dielectric constant variation with temperature measured under different magnetic fields and frequency $f = 50$ kHz. (b) Isothermal magnetodielectric curves [MD $= \frac{\varepsilon(H)-\varepsilon(0)}{\varepsilon(0)}$ in %] at different temperatures. (c) Temperature-dependent pyrocurrent recorded under different magnetic fields with the poling electric field of $E_{pol} = +6.74$ kV/cm. (d) The corresponding electric polarization. (e) P vs H curves at various temperatures. (f) H-T phase diagram (where PM = paramagnetic, AFM = antiferromagnetic, FM = ferromagnetic, PE = paraelectric, and ME = magnetoelectric): for Er_2BaCuO_5.

compound exhibits a pyrocurrent anomaly at T_N^{Er} above 0.9 T. Upon further increasing the magnetic field, we have observed different pyrocurrent anomalies around T_N^{Er}. These anomalies are suppressed at high magnetic fields. The magnetic field dependent polarization is shown in Fig. 4(d) and Fig. 4(e). These low-temperature results are similar to that reported earlier [8]. However, we did not observe high-temperature nonpolar to polar structural transition in our samples. Therefore, the appearance of electric polarization above $H_c \sim 0.9$ T confirms the presence of a polar state arising from the change of magnetic structure. The maximum polarization of 4.7 $\mu C/m^2$ is observed at 1.25 T and 2 K. At different magnetic fields, the appearance of pyrocurrent anomalies reveals that this compound may undergo different magnetic phase transitions with different magnetic symmetries. These magnetic symmetries, in turn, allow magnetoelectric coupling. For brief understanding of these results, we show the H-T phase diagram in Fig. 4(f). These results demonstrate that Er_2BaCuO_5 shows field-induced magnetoelectric properties similar to R_2BaCuO_5 (R = Dy and Ho) and $BaHoFeO_4$ [7,29]. To understand the possible mechanism responsible for the field-induced magnetoelectric coupling and to obtain accurate phase diagram, one must perform the neutron diffraction under magnetic field on single crystals.

1. Magnetic field dependent dc bias magnetoelectric current measurements

Temperature-dependent dc bias current measurements at different fields shown in Fig. 5(a) confirm the intrinsic nature of the electric polarization. In the multiferroic community, this technique has been widely used to find the intrinsic nature of the observed polarization and more details can be found in Supplemental Material [30–32]. In addition to temperature-dependent dc bias measurements, we have carried out magnetic field dependent dc bias measurements [29]. The theory is same for both cases, but the main difference is that we vary the magnetic field in the latter case whereas in the first case we use temperature sweep. As shown in Fig. 5(b), we have recorded the dc bias magnetoelectric current while sweeping the field between −5 to 5 T under the presence of dc electric field $E_{dc} = +6.74$ kV/cm. It shows small but broad polarization and sharp depolarization peaks around the metamagnetic transition replicating the temperature-dependent dc bias current. Further, we have calculated the electric polarization by integrating the dc bias magnetoelectric current with respect to time, which is shown in Fig. 5(c) and the corresponding polarization is provided in Fig. 5(d). Therefore, magnetic field dependent dc bias measurements make evident the absence or presence of magnetoelectric coupling below or above H_c, respectively, in addition to the T-dependent dc bias technique. We confirm that this measurement can be used to find the field-induced ferroelectric transitions with even small values of polarization. Additionally, to examine the magnetoelectric effect, we have carried out the temperature-dependent magnetoelectric current measurements. Prior to the measurement, we have poled the sample in the presence of electric field and magnetic field (–2 T) down to 2 K across the transition temperature T_N^{Er}. Subsequently, we recorded the current by sweeping the magnetic field between −2 to 2 T,

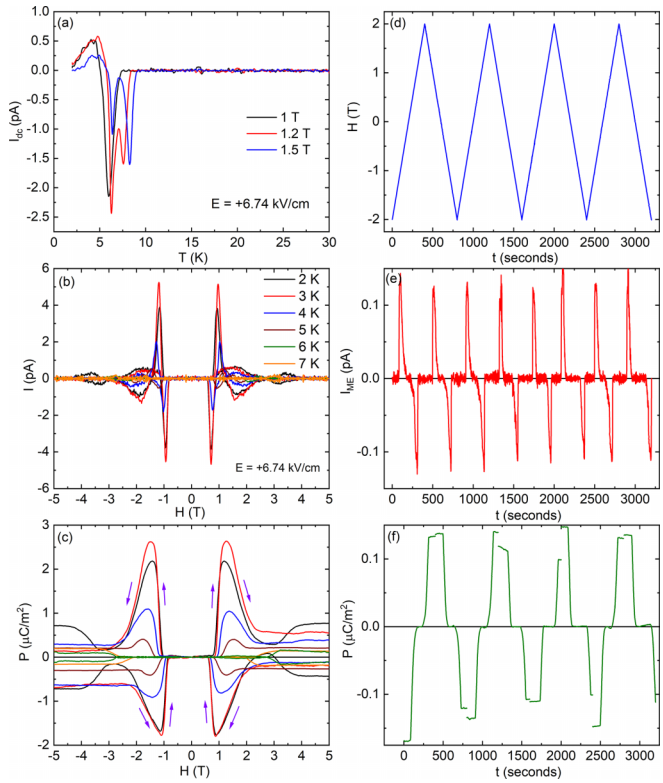

FIG. 5. (a) Temperature-dependent dc bias current measured at different magnetic fields. (b) Magnetic field dependent dc bias magnetoelectric current measured at different temperatures in the loop −5 T to 5 T in the presence of dc electric field $E_{dc} = +6.74$ kV/cm. (c) corresponding electric polarization. (d, e, f) Sweeping of magnetoelectric current measured against the magnetic field at 2 K after the magnetoelectric poling under $E_{pol} = +6.74$ kV/cm and $H = -2$ T.

which is shown in Figs. 5(e)–5(f). It is evident that magnetoelectric current and corresponding polarization oscillates with the magnetic field confirming the strong magnetoelectric coupling.

C. Absence of magnetoelectric coupling in R_2BaCuO_5 (R = Eu, Y, Lu, and Tm)

The magnetic properties of green phase compounds are rich and vary with the R ion due to the intriguing role of the $4f$-$3d$ exchange coupling. In this view, it will be very interesting to study nonmagnetic R ion (Eu, Y, and Lu) to understand the role of the $4f$-$3d$ coupling. The results of Eu_2BaCuO_5 are presented in Fig. 6. This compound exhibits antiferromagnetic ordering of Cu^{2+} moments at $T_N^{Cu} = 16.3$ K and short-range correlations represented by broad anomaly in magnetization data as shown in Fig. 6(a). Specific heat data [Fig. 6(a)] shows a sharp λ-type anomaly at $T_N^{Cu} = 16.3$ K revealing the long-range magnetic ordering. The isothermal magnetization curves show linear behavior indicating an antiferromagnetic coupling as shown in Fig. 6(b). Y_2BaCuO_5 exhibits magnetic ordering of Cu^{2+} spins at $T_N^{Cu} = 15$ K, which is further confirmed by the heat capacity as seen from Fig. 6(c). The broad maximum at 30 K from the magnetic data [see inset of Fig. 6(c)] is due to presence of short-range correlations. From the Curie-Weiss fit [inset of Fig. 6(c)], the effective

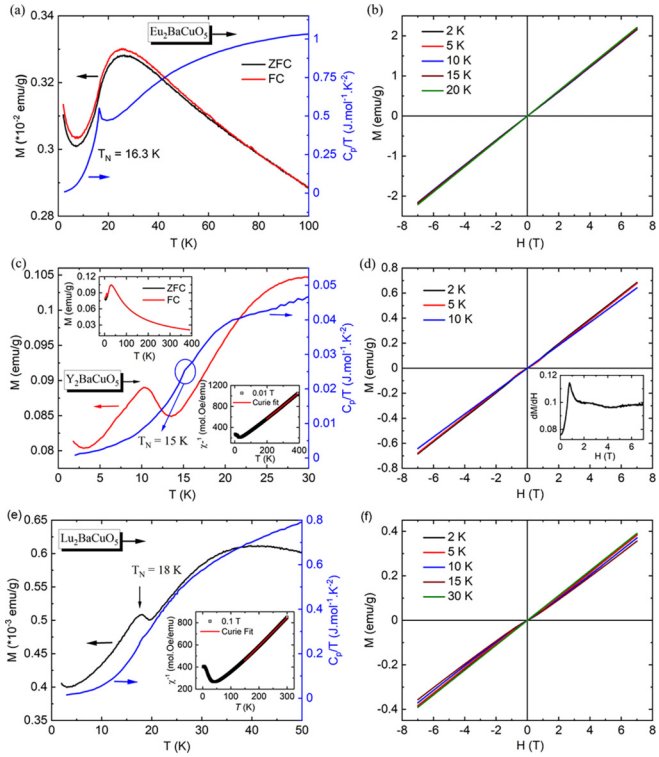

FIG. 6. (a) Left: dc magnetization measured under 0.01 T in zero field-cooled (ZFC) and field-cooled (FC). Right: Specific heat data collected at 0 T. (b) M vs H curves at different temperatures: for Eu_2BaCuO_5. (c) Temperature dependence of magnetization (under 0.01 T) and specific heat (at 0 T). Insets shows (top) ZFC and FC magnetizations in the temperature range 2–300 K and (bottom) inverse susceptibility with Curie-Weiss fit. (d) Isothermal magnetization curves and inset shows dM/dH curve at 2 K; for Y_2BaCuO_5. (e) Left: M vs T measured under magnetic field of 0.1 T in field-cooled protocol. Right: Heat capacity data. Inset shows the inverse susceptibility with Curie-Weiss fit. (f) M vs H data; for Lu_2BaCuO_5.

paramagnetic moment is 1.786 μ_B, which is in good agreement with the theoretical value (1.73 μ_B) of Cu^{2+} ions and the Curie-Weiss temperature $\theta_{CW} = -25.27$ K. The magnetic field dependent magnetization, which is shown in the Fig. 6(d) and its inset, confirms the antiferromagnetic behavior and metamagnetic behavior, respectively. Lu_2BaCuO_5 exhibits anomaly at $T_N^{Cu} = 18$ K in magnetic data [Fig. 6(e)] where the Cu^{2+} spins order antiferromagnetically. Correspondingly, there is a small kink in specific heat data, which further reveals the long-range magnetic ordering. The broad peak around 40 K is indicative of short-range correlations between Cu spins similar to Eu and Y. This behavior is not seen in other compounds due to high paramagnetic moment of magnetic rare-earth metal ions. The effective magnetic moment of 1.76 μ_B confirmed that the Cu indeed is in oxidation state +2. The negative value of $\theta_{CW} = -29.98$ K shows the presence of dominant antiferromagnetic interactions. Further, the isothermal magnetization curves [Fig. 6(f)] suggest an antiferromagnetic ordering between the Cu^{2+} spins. Our dielectric (Fig. S7) and pyrocurrent measurements confirmed the absence of magnetoelectric coupling in all these three compounds [26].

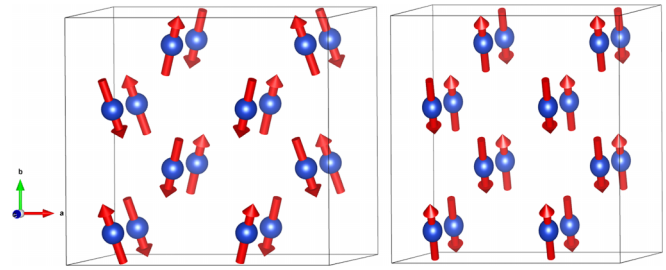

FIG. 7. Schematic of the magnetic structures at 1.5 K for Y_2BaCuO_5 (left) and Lu_2BaCuO_5 (right). In the case of Lu_2BaCuO_5, we have fixed arbitrarily the component m_x to zero, giving rise to a collinear structure.

Additionally, we have carried neutron diffraction measurements on Y_2BaCuO_5 and Lu_2BaCuO_5 compounds to understand the absence of magnetoelectric effect. We did not perform neutron diffraction on Eu_2BaCuO_5 due to high neutron absorption of natural Eu. The Rietveld refined neutron data in the paramagnetic region for Y_2BaCuO_5 is given in Fig. S8 [26]. Both compounds exhibit same magnetic structure with propagation vector $\mathbf{k} = (0, ½, ½)$. We have carried symmetry analysis by using ISODISTORT for the $\mathbf{k}$ vector (0, ½, ½) and paramagnetic space group $Pnma.1'$. There are six possible magnetic models corresponding to the different directions of the order parameter for the irreps mT1 and mT2. The possible magnetic models correspond to different versions of the magnetic space groups: C_amc2_1, P_a2_1/c, and P_a2_1 in BNS notation.

The resolution of the magnetic structure of both compounds is hampered by the weakness of the magnetic contribution of Cu^{2+} ions (1 μ_B is the maximum expected magnetic moment) and the small amount of available sample, especially for the Lu compound that is also absorbing. The orthorhombic solution C_amc2_1 (UNI: $Cmc2_1.1'_a[Pmc2_1]$) fits very well the diffraction pattern of the Y compound but it implies the splitting in two independent sites for Cu^{2+} ions with different moments and, most importantly, it is noncentrosymmetric and should give an electrical behavior that is not observed in the macroscopic measurements. In Figs. S8 and S9, we provide the Rietveld refined neutron data and the magnetic structure described by the Shubnikov group C_amc2_1 for Y_2BaCuO_5 [26].

An equally good fit is obtained for the group P_a2_1/c, coming from the irrep mT1(a, a) in the ISODISTORT notation, with the advantage that, in this case, the magnetic structure is centrosymmetric, and no electrical polarization or magnetoelectricity is allowed, which agrees with the observed macroscopic measurements. We then adopt this solution for both Y and Lu compounds. In spite of the weakness of magnetic reflections, all components of the magnetic moment of Cu^{2+} ions can be freely refined, resulting in a noncollinear magnetic structure. However, the standard deviation of the m_x component is higher than its value, so fixing to zero this component results in a collinear structure with the common axis determined by the ratio between m_y and m_z. Putting $m_x = 0$ is necessary for the case of the Lu compound in order to obtain convergence. In Fig. 7, we represent the magnetic structures of both compounds, and the Rietveld refinements

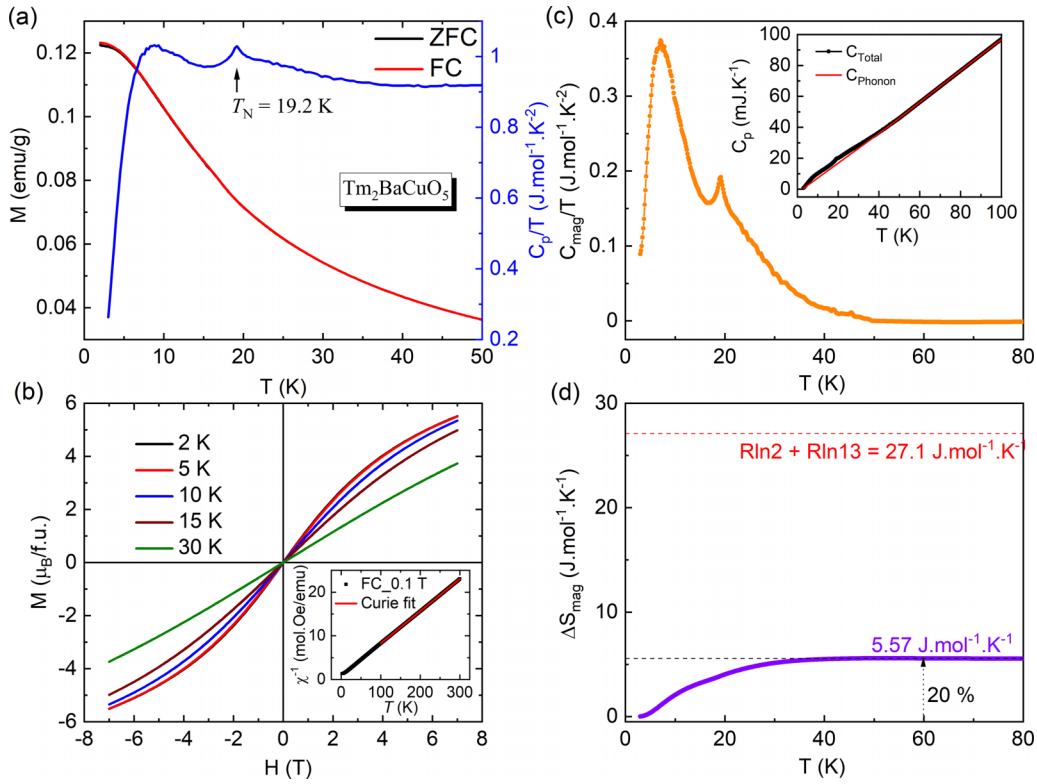

FIG. 8. (a) Left: dc magnetization with respect to temperature measured with 0.01 T under ZFC and FC conditions. Right: Specific heat at constant pressure measured in the absence of magnetic field. (b) M vs H curves recorded at different temperatures. Inset shows the χ^{-1} vs T data; for Tm_2BaCuO_5. (c) Magnetic heat capacity extracted by subtracting the phonon contribution, which is obtained by the Debye-Einstein fitting shown in the inset. (d) Magnetic change in entropy and the corresponding theoretical value are represented in red line.

are represented in Figs. S10 and S11 (see the Supplemental Material for details of the results at 1.5 K in the mCIF files: Y2BaCuO5.mcif and Lu2BaCuO5.mcif) [26]. In support of this, previous spectral studies suggested the same magnetic structures for all these three compounds [20]. In addition, the observed spin structure does not break the inversion symmetry to show magnetoelectric effect, which is consistent with the pyrocurrent measurements. It is noteworthy that the obtained magnetic structure in Y_2BaCuO_5 is different from previously reported findings [23,33]. The previous study proposed two **k** vectors (0, 0, ½) and (½, 0, ½) for the ordered arrangement of Cu sublattice [33]. However, Golosovsky *et al.*, confirmed the correct k vector (0, ½, ½) [23]. Despite this, they indicated ambiguity in determining the spin structure and reported that the structure could be constituted by collinear (along the *c* axis) A-type or F-type modes within a primitive cell, and they mentioned that these two solutions could not be distinguished from their powder neutron diffraction data. In contrast, our investigation reveals a noncollinear AFM spin structure, of type (C_x, G_y, A_z) with dominant G_y component in the notation of Ref. [23], unambiguously described by the Shubnikov group P_a2_1/c, which aligns with the absence of magnetoelectric effect.

Finally, we have shown the results of Tm_2BaCuO_5 in Fig. 8. From Fig. 8(a), the magnetic data did not show any anomaly until down to 2 K. However, heat capacity shows a clear anomaly at $T_N^{Cu} = 19.3$ K where Cu^{2+} spins can be ordered antiferromagnetically. The low-temperature broad anomaly might be due to the Schottky effect associated with crystal field excitations of Tm^{3+} ions. We did not see the corresponding anomaly in magnetic measurements, but this can be due to the high paramagnetic moment of Tm^{3+} ions. Unlike other compounds, the absence of any anomaly below T_N^{Cu} in magnetic data suggests that Tm^{3+} ions did not order until down to 2 K. This different behavior could be related to the anisotropy of the Tm^{3+} ions or to the tendency of this non-Kramers ion to have a singlet ground state in the presence of a crystal field [34,35]. In this compound, we expect that the exchange energy between Tm ions to be lower as compared to crystal field splitting, resulting in the absence of long-range magnetic ordering. To observe the magnetic ordering of Tm ions, the exchange energy must be higher than the gap between the isolated singlet ground state and the first excited state, which may be achieved at very low temperatures. Also, it can be possible that Cu spins would have polarized Tm^{3+} spins below T_N^{Cu} [36]. The M vs H curves [Fig. 8(b)] are not exactly linear as expected for the antiferromagnetic behavior, which might be due to induced moment at Tm site or Tm orders independently below 2 K. There is no metamagnetic transition indicating the Tm^{3+} ions ordering is absent. The effective magnetic moment obtained from the Curie-Weiss fit is 10.414 μ_B, which is consistent with the free ion value (10.816 μ_B) of Tm^{3+} and Cu^{2+} ions. To further confirm the absence of Tm ordering, we analyzed phonon contribution to the heat capacity data using Debye-Einstein fitting, as shown in inset of Fig. 8(c). The magnetic contribution to the heat capacity was obtained by subtracting the phonon contribution, as illustrated in Fig. 8(c). The corresponding magnetic change

TABLE I. Summary of magnetic and magnetoelectric properties of R_2BaCuO_5 (R = Sm − Lu, and Y) [38].

Rare earth (R)	T_N^{Cu} (K)	T_N^R (K)	K vectors $T_N^{Cu} \leqslant T \leqslant T_N^R$ $T < T_N^R$	Magnetic structure	Mag. Symm.	Property	Ref.
Sm	23	5	(0, 0, 0)	–	–	Linear magnetoelectric (LME)	[9]
Eu	16.3	–	–	–	–	Not ME	This work
Gd	11.9	6	(0, 0, g)	Cycloidal	$2mm.1'$	Multiferroic	[6]
			(0, 0, ½)	Noncollinear			
Dy	18.5	10.7	(0, ½, 0)	Noncollinear	$2/m.1'$	LME + Field-Induced	[7]
			(0, 0, 0)	Noncollinear	$mm'm$	Ferroelectric	
Ho	17.5	8	(0, ½, 0)	Noncollinear	$2/m.1'$	LME + Field-Induced	[7]
			(0,0,0) + (0,½,0)	Noncollinear	$2'/m$	Ferroelectric	
Y	15	–	(0,½,½)	Quasi-collinear	$2/m.1'$	Not ME	This work
Er	19.3	5.1	(0,½,0)	Noncollinear	$2/m.1'$	Field-Induced	This work
			(0,½,0)	Noncollinear		Magnetoelectric	
Tm	19.2	–	(0,½,0)	Noncollinear	$2/m.1'$	Not ME	[[19], This work]
Lu	18	–	(0,½,½)	Quasi-collinear	$2/m.1'$	Not ME	This work

in entropy is $\Delta S = 5.57\,J\,mol^{-1}\,K^{-1}$, as depicted in Fig. 8(d), which is close to the theoretical value $R\ln(2S+1) = R\ln 2$ (R is gas constant) of Cu^{2+} spins (S = ½). However, this is only 20% of the total entropy ($R\ln 2 + R\ln 13$) of the compound having Cu^{2+} (S = ½) and Tm^{3+} (J = 6) spins. Hence, this suggests the absence of magnetic ordering of Tm ions.

Interestingly, Tm_2BaCuO_5 shows no magnetoelectric properties, which further confirms the weakness of the $4f$-$3d$ coupling and the absence of Tm ordering. It has been suggested that this compound has a **k** vector equal to (0, ½, 0), like that of Er_2BaCuO_5 [19]. The neutron diffraction experiments in the paramagnetic region confirms the centrosymmetric *Pnma* crystal structure (see Fig. S13) [26]. Below T_N^{Cu}, down to 1.5 K, visually it is difficult to see new peaks corresponding to magnetic ordering; this is due to the low amount of sample used in the experiment. However, if we try to refine the magnetic ordering of Cu^{2+} assuming a structure similar to that of Er_2BaCuO_5, we obtain a value of the magnetic moment of 0.87 (13) μ_B with very high R factor due to the weakness of the reflections and the noise of the experimental data (see Figs. S13 and S14) [26]. The predicted peak positions and intensities are compatible with the observed pattern at 1.5 K. Moreover, the absence of stronger new peaks confirms the absence of ordering of the Tm^{3+} ions ordering. The absence of magnetoelectric coupling in this compound under null or finite magnetic fields suggests the absence of Tm ordering despite the assumed same spin structure as that of Er compound. It is then quite possible that the magnetic structure of Tm_2BaCuO_5 with **k** vector (0, ½, 0) is similar to that (P_b2_1/n) of Dy, Ho, and Er, which is centrosymmetric and does not allow the magnetoelectric coupling (provided Tm2BaCuO5.mcif file as Supplemental Material) [26].

In the discussion, as mentioned earlier, the Er compound exhibits a metamagnetic transition that is absent in other compounds. R_2BaCuO_5 (R = Eu, Y, and Lu) displays antiferromagnetic ordering, where the outermost d electrons of Cu ions participate in the exchange interaction. This exchange is strong and does not change with applied magnetic fields, hence no metamagnetic transition is observed. Tm_2BaCuO_5 does not show magnetic ordering of Tm^{3+} ions, and Cu^{2+} ions alone are responsible for the strong antiferromagnetic interaction, resistant to external magnetic fields. In contrast to these compounds, Er ions undergo ordering due to interactions involving f-f electrons interactions and coupled to d electrons through the magnetic interaction path (Cu^{2+}-O^{2-}-Er^{3+}-O^{2-}-Cu^{2+}). However, the interactions among the f electrons are weak compared to d-d interaction. Therefore, applied magnetic fields influence the magnetic structure through the f-d coupling resulting in the metamagnetic transition.

We summarized all the magnetic and electrical properties of the studied green phases in Table I. From the table, it can be noted that these compounds exhibit a wide variety of magnetic properties along with magnetoelectric coupling. Moreover, R ions did not order down to 2 K in isostructural compounds R_2BaZnO_5 [37]. This suggests the interaction between Cu and R ions is necessary for the ordering of R ions. In most of the green phases, ordering of the magnetic rare-earth metal ion in turn changes the magnetic symmetry and allows the magnetoelectric effect. However, the symmetry below T_N^{Cu} does not allow the coupling between magnetic and electric orders except for R_2BaCuO_5 (R = Sm and Gd). In addition, there are important differences in the ground states for the Dy, Ho, and Er compounds. The low-temperature structure changes to (0, 0, 0) for Dy and (0, 0, 0) + (0, ½, 0) for Ho from high-temperature structure with **k** vector (0, ½, 0) upon R-ion ordering. Both compounds exhibit linear magnetoelectric effect up to magnetic field of ∼1 T and ferroelectric states above their respective metamagnetic transitions. Whereas the structure with **k** = (0, ½, 0) is the same across the Er ordering till down to 1.5 K. This compound shows magnetoelectric states only above $H_c = 0.9$ T. Surprisingly, Tm ions did not order down to 2 K. Though the ground-state magnetic structure of Tm_2BaCuO_5 is like that of Er, it did not show magnetoelectric properties under applied magnetic field. This is due to the absence of Tm order and the absence or weak $4f$-$3d$ coupling. This indicates the importance of R ion and its ordering. Unlike these compounds, the Gd_2BaCuO_5 case is completely

different where it shows the simultaneous ordering of Gd and Cu ions. This is because Gd ground state is S state and the crystalline electric field effects are negligible for this. These compounds have two different sites for R ions and the crystalline electric fields at both sites are different. Each R ion has significant crystal field splitting, which can lead to different magnetic structures. The variation of the number electrons in the $4f$ shell for different R ions leads to a suppression of interactions and ordering in some cases. Therefore, these results suggest the important role of $4f$-$3d$ coupling and single-ion anisotropy of R ions in the observation of magnetoelectric effect.

After examining the magnetic structures of each compound, we can infer that the fundamental microscopic mechanism responsible for magnetoelectricity or multiferroicity likely stem from established phenomena such as exchange striction and/or inverse Dzyaloshinskii-Moriya interaction [2,3]. For instance, in compounds such as R_2BaCuO_5 (where R = Dy and Ho), the linear magnetoelectric effect is likely attributed not only to single-ion anisotropy but also to the influence of exchange striction [7]. Similarly, considering symmetry principles, the magnetoelectric coupling observed in Sm_2BaCuO_5 is likely driven by single-ion anisotropy [9]. However, comprehending the precise mechanism behind the magnetoelectric effect in Sm_2BaCuO_5 necessitates a deeper understanding of its spin structure. On the other hand, the multiferroicity observed in Gd_2BaCuO_5, characterized by an elliptical cycloidal structure, is likely governed by the inverse Dzyaloshinskii-Moriya interaction [6]. To gain a comprehensive understanding of the mechanisms governing the field-induced multiferroic properties in compounds such as R_2BaCuO_5 (where R = Dy, Ho, and Er), it becomes imperative to conduct neutron diffraction experiments on single crystals under varying magnetic fields [7].

IV. CONCLUSION

In summary, we have systematically investigated the magnetic and magnetoelectric properties of R_2BaCuO_5 (R = Er, Eu, Y, Tm, and Lu). Er_2BaCuO_5 exhibits metamagnetic transition at a critical field of $H_c \sim 0.9$ T and a large magnetization of $9\,\mu_B$/f.u. at 7 T and 2 K. Moreover, above H_c, it shows field-induced electric polarization indicating the presence of magnetoelectric coupling. Further, magnetic field dependent dc bias magnetoelectric measurements illustrated to confirm the magnetoelectric effect. In all other compounds, Cu^{2+} ordered antiferromagnetically at T_N^{Cu} = 15–20 K and did not show magnetoelectric properties. Neutron diffraction measurements revealed a strongly noncollinear magnetic structure obtained from **k** vector (0, ½, 0), with magnetic symmetry P_b112_1/n for Er and collinear structure obtained from (0, ½, ½), with magnetic symmetry P_a2_1/c for Y and Lu compounds.

Finally, a comparative analysis of the magnetic and magnetoelectric characteristics of R_2BaCuO_5 compounds (where R ranges from Sm to Lu, including Y) [6,7,9,38] reveals intriguing insights. Specifically, Sm_2BaCuO_5 demonstrates a linear magnetoelectric effect below the Cu-ordering temperature. Compounds such as Dy_2BaCuO_5 and Ho_2BaCuO_5 exhibit a linear magnetoelectric effect below the magnetic ordering temperature of Dy/Ho ions and above the metamagnetic transition, displaying multiferroic properties. Gd_2BaCuO_5 showcases multiferroic properties due to an elliptical cycloidal spin structure, where Gd and Cu moments order at the same temperature. Er_2BaCuO_5 displays multiferroic properties above the metamagnetic transition. Conversely, R_2BaCuO_5 compounds with R being Eu, Y, Tm, and Lu do not display magnetoelectric coupling.

These findings suggest that $4f$-$3d$ coupling plays a crucial role in determining the diverse magnetic structures and magnetoelectric properties within the green phase family of compounds. The variety of magnetic structures underscores the range of multiferroic and magnetoelectric phenomena in this compound family. Notably, the significance of $4f$-$3d$ interactions in dictating the ground-state magnetic structure implies that these materials may garner similar renown to orthorhombic rare-earth manganites $RMnO_3$ and manganates RMn_2O_5, known for their diverse electric polarization directions and magnetic field-induced reorientations.

Furthermore, it is noteworthy that while Mn-O-Mn (d-d)-exchange interactions are solely responsible for multiferroic properties in later compounds, magnetoelectric coupling in green phases results from f-d electron interactions. This underscores the importance of f-d coupling as a novel avenue for designing magnetoelectric and multiferroic materials. Hence, our study confirms the potential of f-d coupling as a promising pathway for developing new magnetoelectric and multiferroic materials.

ACKNOWLEDGMENTS

The authors would like to thank Sheikh Saqr Laboratory (SSL) and the International Centre for Materials Science (ICMS) at Jawaharlal Nehru Centre for Advanced Scientific Research (JNCASR) for various experimental facilities.

[1] T. Kimura, T. Goto, H. Shintani, K. Ishizaka, T. Arima, and Y. Tokura, Magnetic control of ferroelectric polarization, Nature (London) **426**, 55 (2003).

[2] D. Khomskii, Classifying multiferroics: Mechanisms and effects, Physics **2**, 20 (2009).

[3] Y. Tokura, S. Seki, and N. Nagaosa, Multiferroics of spin origin, Rep. Prog. Phys. **77**, 076501 (2014).

[4] P. Yanda and A. Sundaresan, Linear magnetoelectrics and multiferroics, in *Advances in the Chemistry and Physics of Materials* (World Scientific, Singapore, 2019), pp. 224–248.

[5] A. Sundaresan and N. V. Ter-Oganessian, Magnetoelectric and multiferroic properties of spinels, J. Appl. Phys. **129**, 60901 (2021).

[6] P. Yanda, I. V. Golosovsky, I. Mirebeau, N. V. Ter-Oganessian, J. Rodríguez-Carvajal, and A. Sundaresan, Interplay of 4f−3d interactions and spin-induced ferroelectricity in the green phase Gd_2BaCuO_5, Phys. Rev. Res. **2**, 023271 (2020).

[7] P. Yanda, F. Orlandi, P. Manuel, N. Boudjada, J. Rodriguez-Carvajal, and A. Sundaresan, Magnetic-field-induced ferroelectric states in centrosymmetric R_2BaCuO_5 (R = Dy and Ho), Phys. Rev. B **104**, 144401 (2021).

[8] A. Indra, S. Mukherjee, S. Majumdar, O. Gutowski, M. v. Zimmermann, and S. Giri, High-temperature ferroelectric order and magnetoelectric coupling driven by the magnetic field cooling effect in R_2BaCuO_5 (R = Er, Dy, and Sm), Phys. Rev. B **100**, 014413 (2019).

[9] P. Yanda, N. V. Ter-Oganessian, and A. Sundaresan, Linear magnetoelectric effect in antiferromagnetic Sm_2BaCuO_5, Phys. Rev. B **100**, 104417 (2019).

[10] S. Mishra, P. Yanda, and A. Sundaresan, Effect of Nd substitution on magnetoelectric properties of Sm_2BaCuO_5, Bull. Mater. Sci. **43**, 305 (2020).

[11] S. Mishra, P. Yanda, S. Bhat, M. Etter, and A. Sundaresan, High-pressure synthesis and magnetic properties of tetragonal R_2BaCuO_5 (R = Sm and Eu), Front Chem **11**, 1166475 (2023).

[12] A. T. Apostolov, I. N. Apostolova, and J. M. Wesselinowa, Origin of multiferroism in Sm_2BaCuO_5, Solid State Commun. **352**, 114808 (2022).

[13] C. Michel and B. Raveau, Les oxydes A_2BaCuO_5 (A = Y, Sm, Eu, Gd, Dy, Ho, Er, Yb), J. Solid State Chem. **43**, 73 (1982).

[14] A. Salinas-Sanchez, J. L. Garcia-Muñoz, J. Rodriguez-Carvajal, R. Saez-Puche, and J. L. Martinez, Structural characterization of R_2BaCuO_5 (R = Y, Lu, Yb, Tm, Er, Ho, Dy, Gd, Eu, and Sm) oxides by x-ray and neutron diffraction, J. Solid State Chem. **100**, 201 (1992).

[15] J. A. Campá, J. M. G. de Salazar, E. Gutiérrez-Puebla, M. A. Monge, I. Rasines, and C. Ruíz-Valero, Crystal structure of the oxides $BaCuGd_2O_5$ and $Ba_2Cu_3GdO_{7-x}$, Phys. Rev. B **37**, 529 (1988).

[16] K. Kanoda, T. Takahashi, T. Kawagoe, T. Mizoguchi, S. Kagoshima, and M. Hasumi, Antiferromagnetic transition in Y_2BaCuO_5, Jpn. J. Appl. Phys. **26**, L2018 (1987).

[17] R. Z. Levitin, B. V Mill, V. V Moshchalkov, N. A. Samarin, V. V Snegirev, and J. Zoubkova, Two magnetic transitions and metamagnetism in the R_2BaCuO_5 (R = Sm, Eu, Gd, Dy, Ho, Er, Tm, Yb) compounds, J. Magn. Magn. Mater. **90**, 536 (1990).

[18] V. V Moshchalkov, N. A. Samarin, I. O. Grishchenko, B. V Mill, and Z. J., Magnetic interactions in R_2BaCuO_5 (R =Y, Sm, Eu, Gd, Dy, Ho, Er, Tm, Yb, Lu) compounds, Solid State Commun. **78**, 879 (1991).

[19] I. V. Golosovskii, V. P. Plakhtii, V. P. Kharchenkov, J. Zoubkova, B. V. Mill, M. Bonnet, and E. Roudaut, Magnetic and crystal structures of rare-earth Re_2BaCuO_5 cuprates, Sov. Phys. Solid State **34**, 782 (1992).

[20] I. V Paukov, M. N. Popova, and B. V Mill, Spectral studies of magnetic ordering in the cuprates R_2BaCuO_5 (R = Sm, Eu, Tm, Yb, Lu), Phys. Lett. A **169**, 301 (1992).

[21] K. Tagaya, ESR study of Ln_2BaCuO_5 (Ln = Sm, Eu, Gd, Dy, Yb), J. Magn. Magn. Mater. **104**, 561 (1992).

[22] T. Kobayashi, H. Katsuda, K. Hayashi, M. Tokumoto, and H. Ihara, Single crystal ESR Study of Y_2BaCuO_5, Jpn J Appl Phys **27**, L670 (1988).

[23] I. V. Golosovsky, P. Böni, and P. Fischer, Magnetic structure of Y_2BaCuO_5, Solid State Commun. **87**, 1035 (1993).

[24] A. K. Ovsyanikov, I. V. Golosovsky, I. A. Zobkalo, and I. Mirebeau, Magnetic structure and phase transitions in the "green phase" $^{160}Gd_2BaCuO_5$: Neutron diffraction study, J. Magn. Magn. Mater. **353**, 71 (2014).

[25] J. Rodriguez-Carvajal, FullProf: A Program for Rietveld Refinement and Pattern Matching Analysis, in Abstracts of the Satellite Meeting on Powder Diffraction of the XV Congress of the IUCr, Toulouse, France (1990), p. 127. See also, Physica B **192**, 55 (1993). The FullProf Suite can be freely downloaded from https://www.ill.eu/sites/fullprof.

[26] See Supplemental Material at http://link.aps.org/supplemental/10.1103/PhysRevB.109.104411 for details of the refinement of x-ray diffraction, neutron diffraction, and dielectric measurements. To visualize the magnetic structures, mcif file are provided separately.

[27] H. T. Stokes, D. M. Hatch, B. J. Campbell, and D. E. Tanner, ISODISPLACE: A web-based tool for exploring structural distortions, J. Appl. Crystallogr. **39**, 607 (2006).

[28] B. J. Campbell, H. T. Stokes, J. M. Perez-Mato, and J. Rodriguez-Carvajal, Introducing a unified magnetic space-group symbol, Acta Crystallogr., Sect. A **78**, 99 (2022).

[29] R. Kumar and A. Sundaresan, Unveiling a hidden multiferroic state under magnetic fields in $BaHoFeO_4$, Phys. Rev. B **107**, 184420 (2023).

[30] C. De, S. Ghara, and A. Sundaresan, Effect of internal electric field on ferroelectric polarization in multiferroic $TbMnO_3$, Solid State Commun. **205**, 61 (2015).

[31] N. Terada, Y. S. Glazkova, and A. A. Belik, Differentiation between ferroelectricity and thermally stimulated current in pyrocurrent measurements of multiferroic MMn_7O_{12} (M = Ca, Sr, Cd, Pb), Phys. Rev. B **93**, 155127 (2016).

[32] R. Kumar and A. Sundaresan, Role of dipole relaxation in measuring electric polarization in type-II multiferroics, Z Anorg Allg Chem **649**, e202300074 (2023).

[33] T. Chattopadhyay, P. J. Brown, U. Köbler, and M. Wilhelm, Evidence for the antiferromagnetic ordering of the green phase Y_2BaCuO_5, Europhys. Lett. **8**, 685 (1989).

[34] B. R. Cooper, Magnetic properties of compounds with singlet ground state: exchange correlation effects, Phys. Rev. **163**, 444 (1967).

[35] B. R. Cooper and O. Vogt, Singlet ground state magnetism, Le Journal De Physique Colloques **32**, C1-958 (1971).

[36] G. A. Stewart and P. C. M. Gubbens, Induced thulium magnetisation in the green phase-Tm_2BaCuO_5, J. Magn. Magn. Mater. **206**, 17 (1999).

[37] G. F. Goya, R. C. Mercader, M. T. Causa, and M. Tovar, Magnetic properties of *Pnma*-oxides (R = Sm, Eu, Dy and Ho), J. Phys.: Condens. Matter **8**, 8607 (1996).

[38] P. Yanda and A. Sundaresan, Ph.D thesis, Jawaharlal Nehru Centre for Advanced Scientific Research, 2021, https://libjncir.jncasr.ac.in/xmlui/handle/123456789/3229.